2D Materials

Real-time detection of hepatitis B surface antigen using a hybrid graphene-gold nanoparticle biosensor

To cite this article: F Walters *et al* 2020 *2D Mater.* **7** 024009

2D Materials

OPEN ACCESS

RECEIVED
17 October 2019

REVISED
13 January 2020

ACCEPTED FOR PUBLICATION
6 February 2020

PUBLISHED
5 March 2020

PAPER

Real-time detection of hepatitis B surface antigen using a hybrid graphene-gold nanoparticle biosensor

F Walters[1], S Rozhko[2], D Buckley[2], E D Ahmadi[1], M Ali[1], Z Tehrani[1], J Mitchell[1], G Burwell[3], Y Liu[4,5], O Kazakova[2] and O J Guy[1,6]

[1] Centre for NanoHealth, College of Engineering, Swansea University, Swansea, SA2 8PP, United Kingdom
[2] National Physical Laboratory, Quantum Metrology Institute, Teddington, Middlesex, TW11 0LW, United Kingdom
[3] Department of Physics, College of Science, Swansea University, Swansea, SA2 8PP, United Kingdom
[4] Key Laboratory of Optoelectronic Technology & Systems, Chongqing University, Ministry of Education, Chongqing 400044, People's Republic of China
[5] Centre for Intelligent Sensing Technology, College of Optoelectronic Engineering, Chongqing University, Chongqing 400044, People's Republic of China
[6] Department of Chemistry, College of Science, Swansea University, Swansea, SA2 8PP, United Kingdom

E-mail: O.J.Guy@swansea.ac.uk

Keywords: graphene, hepatitis, gold nanoparticle, biosensor, ssDNA, detection, AFM-IR

Supplementary material for this article is available online

Abstract

A hybrid biosensor based on a graphene resistor functionalized with self-assembled Graphene-AuNPs (Gold Nanoparticles) is demonstrated for the real-time detection of hepatitis B surface antigen (HBsAg). The hybrid biosensor consists of a ssDNA sequence attached to a graphene resistor device via π–π stacking interactions in combination with a ssDNA functionalized AuNP. The ssDNA has complementary sequences which through hybridization, yield the graphene-AuNP hybrid biosensor. Real-time 2-point resistance measurements, performed using varying concentrations of HBsAg, show a linear dependence of resistance change against the logarithm of HBsAg concentration (log[HBsAg]). A limit of detection of 50 pg ml^{-1} was observed. Moreover, the hybrid biosensor platform has potential to be applied to any biomarker of interest.

1. Introduction

Point-of-care (POC) diagnostics have been widely utilized for disease detection as they are fast, cheap and easy to use when compared to laboratory tests, which require highly trained staff, large/expensive equipment and can take several days to receive results [1]. These drivers have spurred rapid growth of POC diagnostic products in recent years with POC tests being particularly desirable in resource-limited settings [2], where convenient, rapid and widespread testing is required.

Rapid diagnosis in resource-limited settings is particularly relevant to diagnosis of hepatitis—a major global health problem affecting almost 400 million people worldwide [3]. Hepatitis B virus (HBV) is a leading cause of liver disease and hepatocellular carcinoma (HCC), with almost 800 000 deaths attributed to HBV and related complications each year [4, 5]. In this work, a sensor for detection of the HBV has been developed, using the established biomarker for HBV acute or chronic infection: hepatitis B surface antigen (HBsAg).

Graphene, with its high conductivity, large surface area and high electron transfer rate has been researched as a platform for electrical, electrochemical & other biosensing [6].

To produce an affinity graphene biosensor, the graphene surface needs to be bio-functionalized for specific biomarker detection [7]. First, the graphene surface must be modified with binding moieties able to attach a specific bioreceptor [8]. This can be achieved by using covalent (covalent bonds between radicals and the C = C bonds of pristine graphene [9], polymerization, cycloadditions or single-atom introductions [10, 11]) or non-covalent methods (electrostatic interactions, π–π stacking or Van de Waals interactions [12]). Specifically, in this work, non-covalent func-

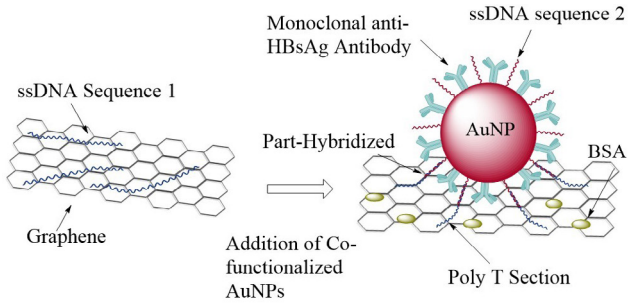

Figure 1. Graphene-AuNP hybrid: AuNPs co-functionalized with monoclonal anti-HBsAg antibody and ssDNA sequence 2 incubated with the ssDNA functionalized (sequence 1) graphene. The part-sequence is hybridized to dsDNA while poly T section remains π–π stacked to the graphene, anchoring the particle to the surface.

tionalization was achieved via π–π stacking of single-stranded deoxyribonucleic acid (ssDNA) to the graphene surface.

DNA nucleobases are able to interact with graphene via π–π stacking interactions, between the ring structures in the nucleobases and the graphene hexagonal units [13], as well as electrostatic interactions of DNA with the basal planes of graphene [12, 14]. Following successful functionalization of the graphene surface, bio-functionalization—attaching bioreceptors such as aptamers, antibodies, enzymes or mRNA probes—can be used to produce specific biosensors. Graphene is highly sensitive to environmental changes and surface modifications. However, this also means it is highly sensitive to entities other than the target analyte, e.g. buffer solutions/complex matrices such as serum and water or other solvents. Therefore, background signals from the test solution can be high and potentially obscure the binding events of specific bioreceptor-target interactions. To enhance the signal from target-sensor interactions, gold nanoparticles (AuNPs) can be added to the sensor to create graphene-AuNP hybrids. The AuNPs provide increased surface area for receptor binding and increased deflection angle of the bioreceptors, potentially reducing steric hindrance when compared to a planar surface, leading to amplified signals and higher sensitivity. Graphene–AuNP hybrid structures are of particular interest in biosensing applications because they display individual properties of graphene and AuNPs, but can also exhibit additional synergistic properties [15]. The presence of AuNPs on a graphene electrode facilitates a conductive interface with a large surface area, increased charge density and excellent biocompatibility [16], promoting charge transfer at the ssDNA modified graphene interface [17]. Here we explore the use of graphene-AuNP hybrids in a real-time 2-point resistance measurement sensor for the detection of HBsAg.

Direct immobilization of biomolecules (e.g. proteins) onto graphene has been reported to be unstable, with frequently applied washing steps during biosensor fabrication readily removing proteins [18]. Graphene decorated with AuNPs may suffer from these same issues if the AuNPs are simply physisorbed. Therefore, a more permanent, stronger and/or targeted attachment of the AuNPs to the graphene surface is required for biosensing applications. Decoration of graphene to produce graphene-AuNP hybrids can be achieved with either *in situ* (physical vapour deposition, electrochemical & hydro-thermal synthesis [18]) or *ex situ* methods. In the *ex situ* approach, nanoparticles are synthesized in advance and subsequently decorated onto the surface of graphene [18], linked by either covalent or noncovalent interactions [19]. Self-assembly of graphene-AuNP hybrids using *ex situ* methods have advantages over *in situ* methods owing to more controlled particle size distribution and more monodisperse surface coverage [20]. The decoration was achieved here through an *ex situ* approach. The π–π stack binding energies are strong enough to form at room temperature, higher binding energies between π–π stacked ssDNA and graphene when compared to that of H-π interactions between water molecules, negate solvent effects [21] and the graphene-AuNP hybrids can be manufactured in aqueous media, under ambient conditions.

In this work, the AuNPs are pre-functionalized with both monoclonal anti-HBsAg antibodies and a thiol modified ssDNA sequence. The AuNPs are then tethered to the graphene surface via DNA oligonucleotide hybridization with part of a complementary ssDNA sequence—the other part of which is bound to the graphene substrate via π–π stacking (figure 1). The AuNPs anchored to the graphene surface constitutes the graphene-AuNP hybrid biosensor, which can be utilised for HBsAg detection. This methodology could be applied to any bioreceptor, making it an interchangeable and potentially universal platform for sensing applications.

2. Materials and methods

2.1. Materials

Graphene on 300 nm thermal oxide SiO_2/Si wafers supplied by Graphenea. Photoresists: Microchem LOR 3A positive photoresist; Microposit S1805 G2 Positive resist; Microposit MF-CD-26 developer and

Microposit Remover 1165 purchased from DOW Electronics Materials. Dielectric paste supplied by Sun Chemical Corporation D1240114D5. Gold nanoparticles (60 nm) purchased from BBI Solutions Ltd.

All ssDNA sequences purchased from Eurogentec. Monoclonal anti-HBsAg & HBsAg analyte purchased from Hytest Ltd. OMNIPUR® DEPC treated water (nuclease- free) purchased from Sigma Aldrich company Ltd. Bovine serum albumin purchased from Sigma Aldrich company Ltd. Phosphate buffered saline purchased from Fisher Scientific UK Ltd. All other reagents purchased from sigma Aldrich Company Ltd and were of analytical grade.

All ssDNA sequences were diluted to stock concentration in OMNIPUR® nuclease-free water and stored at −20 °C before use.

2.2. Graphene device manufacture

Graphene resistor devices were fabricated using CVD (chemical vapour deposited) monolayer graphene on 300 nm thermal oxide SiO_2/Si wafers (p-type, ⟨1 0 0⟩-oriented). Devices consisted of a patterned graphene channel connected at either end to a stacked Cr/Pd metal contact. The graphene channels were patterned using photolithography and subsequently etched using an O_2 plasma. The metal contacts were deposited using physical vapour deposition, 30 nm Cr & 200 nm Pd (using a Kurt J Lesker PVD75). The metal electrodes were passivated using screen-printed dielectric ink, with a window in the passivation layer, enabling exposure of the graphene channel. Details of device manufacture and passivation can be found in supplementary information.

2.3. Graphene-AuNP hybrid manufacture

60 nm AuNPs were co-functionalized, firstly with monoclonal anti-HBsAg antibody by physisorption and secondly, using a thiol modified ssDNA sequence (sequence 2: 5′ SH-TTTTTTTTTCGGATTCTAGAAATTCTTAACTATTTAATC 3′) attached to the AuNPs using S–Au bonding. 10% tween 80 solution was added to 1 ml of OD 1 (Optical Density of 1) AuNP/monoclonal anti-HBsAg conjugate and incubated at room temperature for 30 min. The salt content of the solution was increased to a final concentration of 0.1 M with PBS, followed by the addition of sequence 2 ssDNA, incubating at 50 °C for 1 h 20 min [22]. Excess antibody and ssDNA were removed by centrifugation (4000 rcf for 3 min). The supernatant was removed, and the pellet was resuspended in 1 × PBS (pH 7.4) to ~10 × concentration. The ssDNA sequence (sequence 1: 5′ TTTTTTTTTTTTTTTTTTTTTTTTTTTTTTGATTAAATAGTTAAGAATTTCTAGAATCCG 3′) used to functionalize the graphene resistor device, was dropped on to the graphene channels (20 μl of 100 μM solution in nuclease-free water) and incubated overnight at 2–8 °C. Samples were then washed multiple times in 1 × PBS buffer (pH 7.4) to remove any excess ssDNA. The wash step consisted of 200 μl of PBS buffer (pH 7.4), delivered via pipette and gently dried with nitrogen (N_2), repeated three times. The ssDNA sequence 1 is 60 nucleobases in length. This length was chosen to enable the poly T (poly thymine) section of the sequence to π–π stack on to the graphene surface, while the remaining part-sequence is available for hybridization with sequence 2 bound to the AuNP. Hybridization of the two ssDNA part sequences to ds-DNA (double stranded DNA) tethers the AuNP to the graphene surface. Computational studies have investigated the binding energies of individual nucleobases in order to determine the strength of interaction of the different nucleobases with graphene [23].

It has been demonstrated that a poly A (poly Adenine) sequence can form spherical particles on the graphene surface whereas poly T remains flat [24]. Hence, a poly T part-sequence was used to π–π stack to the graphene surface. The other portion of sequence 2 consisted of a 30-nucleobase length, bound at its thiol termination to the AuNPs. This 30-base part sequence was chosen as it is long enough to hybridize with sequence 1 on the graphene surface but short enough not to hinder the binding capability of the monoclonal anti-HBsAg antibody also present on the AuNP surface. Hybridization of graphene-bound ssDNA sequence 1 with the sequence 2 ssDNA-AuNP, yielding a dsDNA structure, increases the number of nucleobases in the vicinity of the graphene channel and also detaches the bases from the surface of graphene [25]. Both situations will affect the level of doping of the graphene channel, caused by the nucleobases and also by the bound AuNP conjugate.

The AuNP/monoclonal anti-HBsAg/ssDNA functionalized conjugate was diluted to OD2 in PBS (pH 7.4) and incubated on the ssDNA (sequence 1) functionalized graphene for 2.5 h at room temperature. Samples were washed with PBS (pH 7.4) as described above. Bovine serum albumin (BSA) was used to block any remaining sites on the graphene surface to avoid non-specific binding, using a 1% BSA solution (in deionized water) incubated on the graphene surface for 30 min at room temperature. Excess BSA was removed by washing with PBS (pH 7.4).

2.4. Real-time 2-point resistance measurements

Graphene resistor devices with three CVD single-layer graphene channels on a SiO_2/Si substrate were used for sensitive real-time 2-point resistance measurements. A connector (supplied by Biovici Ltd) was used to provide electrical connections between graphene channels and measurement instruments (Supplementary Information, figure S1 & S5 (stacks.iop.org/TDM/7/024009/mmedia)). All three graphene channels were measured simultaneously using a standard lock-in technique. Current- fixed and voltage-fixed measurement regimes were used throughout. Currents of 0.1 or 1.0 μA were passed through the channels in a current-fixed regime. Fixed

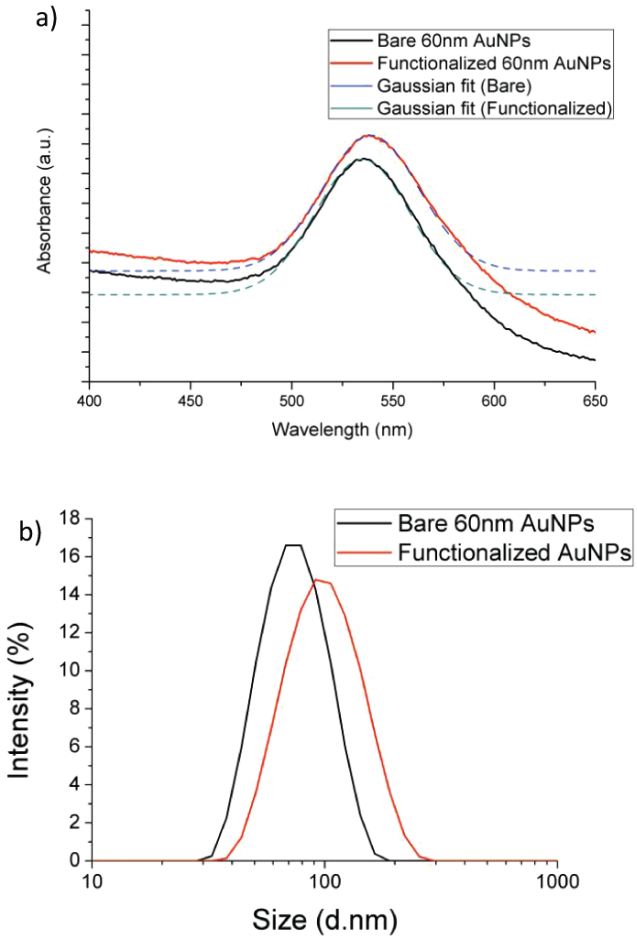

Figure 2. (a) UV–vis absorption spectra for bare 60 nm AuNPs (black) and monoclonal anti HBsAg/ssDNA co-functionalized 60 nm AuNPs (red) (b) DLS distribution by intensity for bare AuNPs (black) and monoclonal anti- HBsAg/ssDNA co-functionalized 60 nm AuNPs (red). Results obtained from an average of 3 measurements consisting of 13 runs per measurement.

voltages of 0.1 or 4 mV were applied to the channel contacts when the voltage-fixed regime was used. The obtained values of the resistances were insensitive to the measurement method. All measurements were performed in ambient conditions (temperature 20 °C, and at normal atmospheric pressure).

3. Results & discussion

3.1. Characterization of functionalized AuNPs

A UV–vis absorption scan was carried out using a BMG LABTECH FLUOstar Omega Microplate Reader at wavelengths between 450–650 nm, with measurements taken at 1 nm intervals. Absorbance spectra were measured for bare 60 nm AuNPs and functionalized 60 nm AuNPs (figure 2(a)).

The UV–vis absorbance spectra show a slight red-shift of the peak absorbance (λ_{max}) after co-functionalization with monoclonal anti-HBsAg and ssDNA sequence 2 ($\lambda_{max} = 535$ nm for bare 60 nm AuNPs and 539 nm for functionalized AuNPs). The red-shift in λ_{max} is due to a change in the local refractive index owing to the attachment of antibody & ssDNA to the particle surface. The λ_{max} shift observed is comparable to those reported in the literature [26, 27], which can be used to confirm antibody attachment to the particle surface [28]. The spectra for the functionalized AuNPs is also slightly broader when compared to bare AuNPs, also indicating attachment of materials to the surface [29].

Dynamic light scattering (DLS), carried out using a Malvern Nano ZS Zetasizer, showed an increase in hydrodynamic diameter (DH) between bare and functionalized AuNPs (figure 2(b)). The DH increased from 65.09 ± 0.27 nm to 91.61 ± 0.82 nm, confirming the attachment of monoclonal anti-HBsAg and ssDNA to the AuNP surface. This increase in DH is consistent with literature values [29]. Low poly dispersity index (PdI) values and the presence of only one peak (see supplementary information) indicates the functionalized AuNPs are not aggregated and are stable in solution. Verification of ssDNA attachment to AuNPs was carried out using a lateral flow assay, results can be seen in supplementary figure S4.

3.2. Characterization of graphene-AuNP hybrids

Raman spectroscopy using a 532 nm excitation was performed on the graphene channels at each stage of functionalization (pristine graphene, ssDNA (sequence 1) functionalized, hybridization with

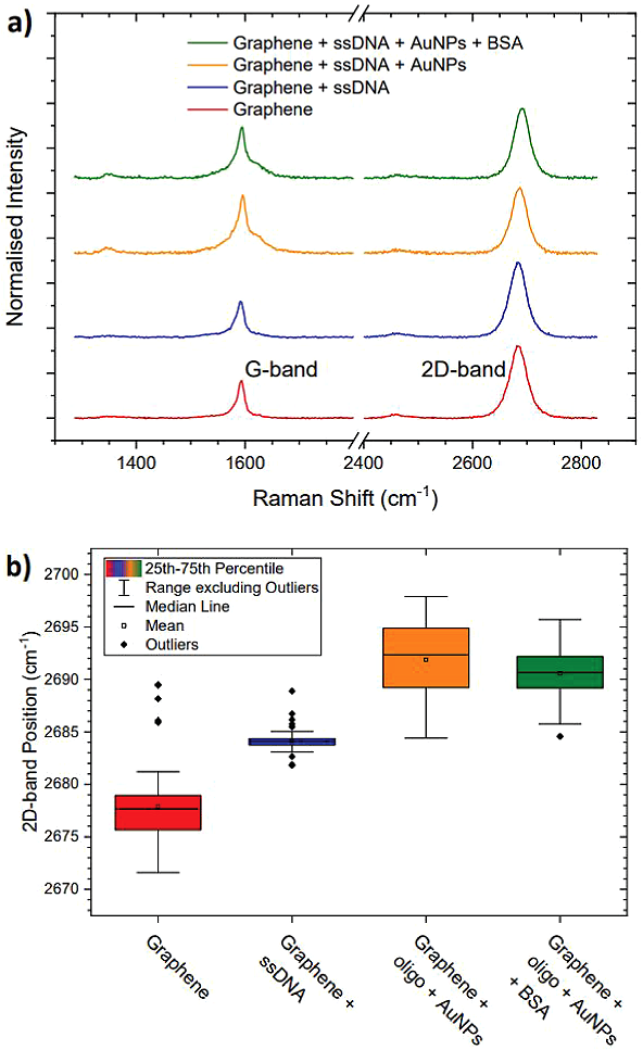

Figure 3. (a) Raman spectra for each functionalization stage. (b) Boxplot of 2D mode positions for each functionalization stage.

co-functionalized AuNP, and final BSA blocking). Mapping scans across the graphene channel were taken, with 104 scans obtained across a 120 × 70 μm area. Representative spectra are shown in figure 3(a). The Raman spectrum of the pristine graphene channel is similar to that of pristine graphene reported in the literature [30], with a G-mode at ~1590 cm^{-1} and 2D mode at ~2700 cm^{-1}. The intensity ratio of these two peaks ($I^{2D}/I^{G} = \sim 2$), as well as the full width half maxima of the 2D mode peak (FWHM2D = 18) indicate that the graphene is a monolayer [31].

The 2D mode for all spectra collected were fitted with a Lorentzian curve and the position of the peaks taken from the fitted data. Figure 3(b) shows a boxplot of the 2D peak positions at each step of the functionalization process. The pristine graphene shows a 2D mode distribution with an average of 2677 cm^{-1}. Four outliers are observed and are attributed to defects and polymer contamination affecting the local graphene electronic and vibrational structure [32]. The mean peak position shifts from the 104 spectra significantly after functionalization with ssDNA to 2684 cm^{-1}, with further, more subtle shifts to 2692 cm^{-1} upon introduction of the AuNPs. Introduction of the blocker BSA shifts the peak slightly in the opposite direction, to 2690 cm^{-1}. This is consistent with doping via electron transfer to the graphene and agrees with the resistance measurements shown in figure 7.

The graphene channel prior to functionalization has p-type conductivity. Slight n-doping via electron donation from the ssDNA reduces the conductivity, and a further reduction is observed after functionalization with the AuNPs. The slight recovery of the conductivity upon introduction of the BSA could be due to some of the AuNPs/ssDNA being washed off the surface during the final washing step.

AFM-IR, a form of photothermal chemical characterization was performed on two samples, an unfunctionalized graphene channel and a channel after decoration with AuNPs and ssDNA. Samples were scanned topographically to determine regions of interest (figure 4) and spectra (850–1200 cm^{-1}) were obtained (figure 5) for functional material on the surface before the sample was rescanned, whilst excited at the wavelength of interest, in this case 1100 cm^{-1}, and an AFM-IR intensity map obtained.

From the spectra in figure 5, the pristine channel shows peaks around 1020–1034 cm^{-1}, attributed to

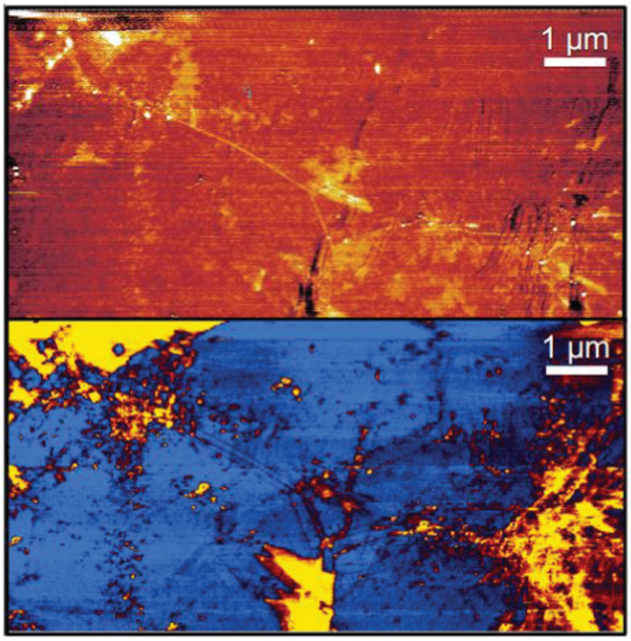

Figure 4. Top: Topography of a ssDNA/AuNP coated graphene channel. Bottom: AFM-IR amplitude scan of the same area, with IR excitation at 1100 cm^{-1}.

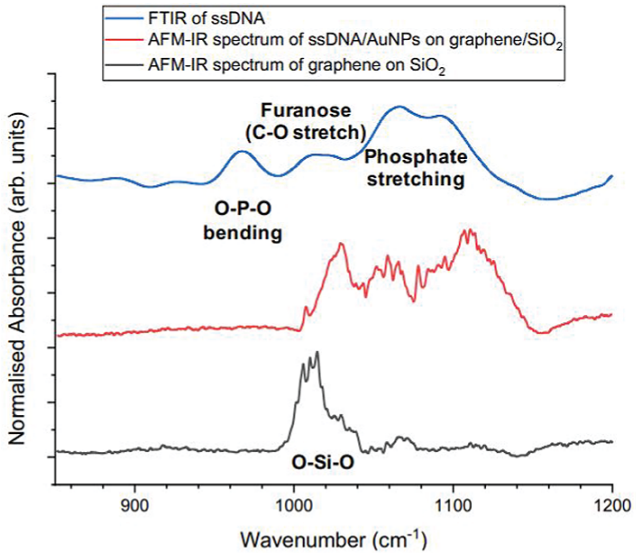

Figure 5. FTIR and AFM-IR spectra of ssDNA and non-functionalized and ssDNA-functionalized graphene.

the underlying SiO_2 substrate. Upon introduction of the AuNPs and ssDNA, these peaks are suppressed in favour of peaks at 1060 cm^{-1} and 1110 cm^{-1}. Comparing to an FTIR spectrum of an aqueous dispersion of ssDNA, the peaks were attributed to the ssDNA phosphate stretching modes [33]. A further peak at 1030 cm^{-1} is assigned to the C–O in the furanose group in the ssDNA—as seen in the FTIR spectrum [34]. A peak at 960 cm^{-1} in the FTIR is attributed to O–P–O bending [33] which is not present in the AFM-IR spectra due to the requirements on the technique for thermal expansion for chemical detection. However, the appearance of the furanose (a five-member ring of four carbons and one oxygen) and phosphate stretching peaks indicate that ssDNA is present on the surface of the graphene channel, demonstrating successful functionalization. A decrease of the I^{2D}/I^{G} ratio, combined with a blueshift of the 2D mode suggests charge transfer to the graphene layer.

An intensity map of absorption at 1100 cm^{-1} shows the distribution of functional material on the surface, with aggregation clearly visible, creating a heterogeneous covering on the graphene channel. This is in agreement with the large range of the Raman 2D mode positions for this sample, as doping via surface moieties causes local electronic perturbations of the graphene. Areas of graphene, not covered by functional material, show smaller shifts of the 1100 cm^{-1} peak.

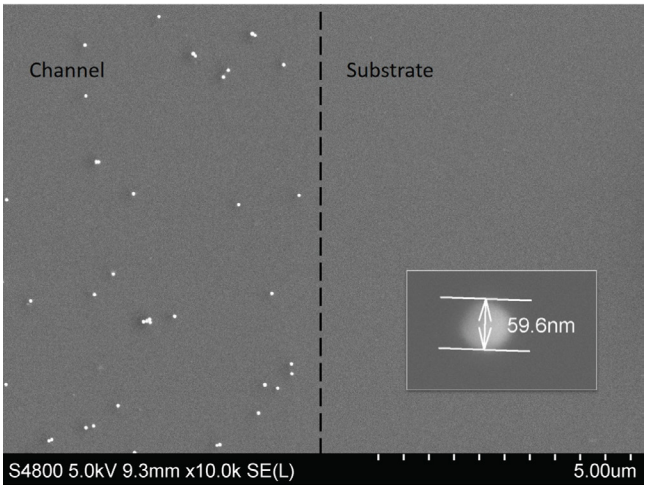

Figure 6. SEM imaging of AuNPs on graphene (a) AuNP attachment to graphene channel versus substrate (image taken at the edge of the graphene channel). (Inset) Measurement confirms the AuNP size as 60 nm.

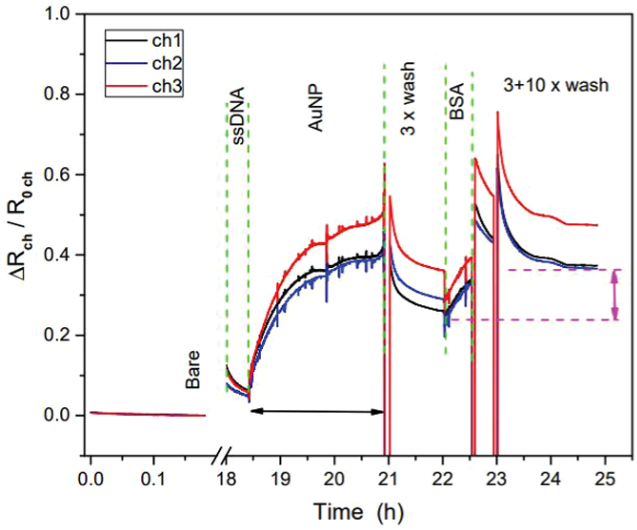

Figure 7. Real-time channel resistance measurements of graphene functionalization process. Where $\Delta R = R_{\text{channel}} - R_0$, and R_0 is the initial resistance measurement.

SEM images (figure 6) show even particle distribution on the graphene surface and indicates that the particles attach to the functionalized graphene only and not to the surrounding SiO_2 substrate.

Validation of antibody/antigen binding and attachment of monoclonal anti-HBsAg to AuNPs was carried out using a lateral flow assay (see figure S3).

3.3. Real-time 2-point resistance measurement of surface functionalization

Real-time 2-point resistance measurements at each stage of graphene functionalization are shown in figure 7.

Real-time resistance measurements, including relaxation periods which may be associated with charge redistribution of the graphene between the charges related to the surface absorbates on one side and those related to the SiO_2/Si substrate on the other [35], were performed on all three graphene channels which show similar behaviour. Each functionalization stage shows an increase in resistance after relaxation when compared to the previous functionalization stage. A significant difference in channel resistance between the ssDNA (sequence 1) stage and the monoclonal anti-HBsAg/ssDNA functionalized AuNP stage is observed. The final resistance, after BSA and final wash steps, also shows this trend of increased resistance compared to the initial baseline.

Measurements using the same electrical conditions were also carried out with a physisorbed control sample, where the graphene surface was not functionalized with ssDNA prior to addition of the AuNP/monoclonal anti-HBsAg/ssDNA functionalized particles. Channel resistances, $\Delta R_{ch}/R_{0\ ch}$, were monitored for

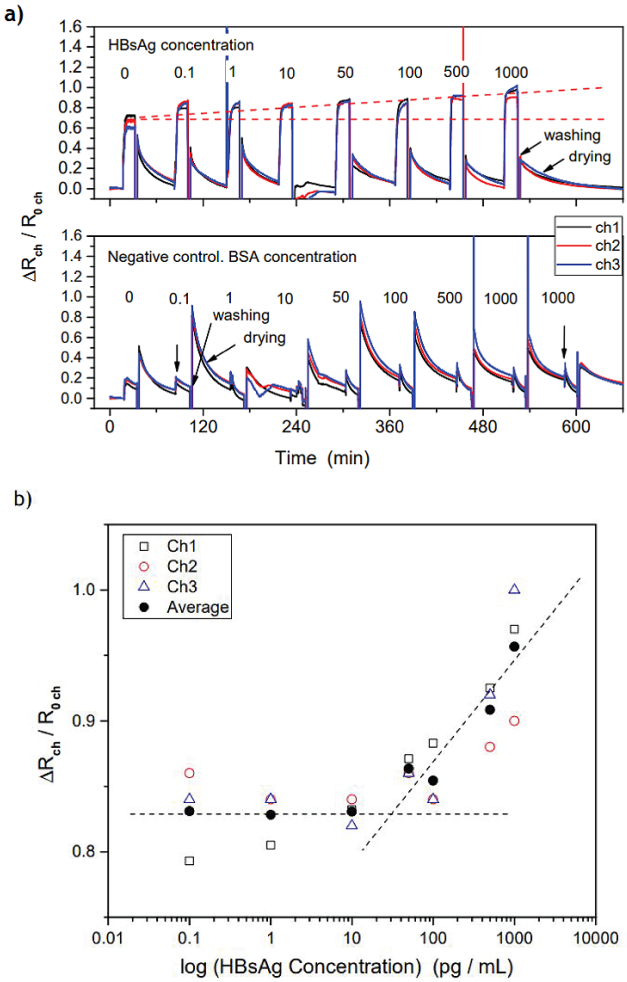

Figure 8. (a) Graphene channel resistance response with respect to the time- dependent application of various HBsAg concentrations in pg ml^{-1} (top) and at various BSA concentrations in pg/ml (bottom). Where $\Delta R = R_{\text{channel}} - R_{0\ \text{channel}}$, and $R_{0\ \text{channel}}$ is the initial resistance measurement. (b) Normalized graphene channel resistance against log HBsAg concentration. An experimental limit of detection (LOD) was measured as an increase of the resistance above this horizontal region at >50 pg ml^{-1}.

each functionalization and wash steps (figure S6). Successful decoration of the graphene with receptors specific to HBsAg thus allows for sensing to be performed.

3.3.1. Real-time 2-point electrical detection of HBsAg

HBsAg sensing was performed using sequential measurements with increasing HBsAg (molecular weight ~24 000 Da) concentration on the same graphene resistor device. Each concentration measurement consisted of a 20 μl droplet of HBsAg (diluted in 1 × PBS (pH 7.4)) solution with increasing concentrations between 0–1000 pg ml^{-1}, placed on the channel window of the functionalized graphene device. This exposed device was incubated for 15 min at room temperature, followed by standard washing (as detailed in the methods section). The functionalized channels were allowed to relax for 45 min and the resistance was monitored in real-time throughout this process. After relaxation, a droplet with higher HBsAg concentration was applied and the resistance change of the device monitored. Figure 8(a) (top) shows the resistance responses, $\Delta R_{\text{ch}}/R_{0\ \text{ch}}$, with respect to varying HBsAg concentrations. It was observed that the $\Delta R_{\text{ch}}/R_{0\ \text{ch}}$ signal reached a level of 0.6 even at 0 pg ml^{-1} concentration (indicating a background response of the graphene channel device to the test buffer solution) of HBsAg, with a gradual increase in resistance with increasing HBsAg concentration. The concentration sensitive area in the response signal is marked by dashed lines in figure 8(a) (top).

Background signal responses in graphene devices can be affected by both intrinsic, e.g. grain boundaries in CVD grown graphene, and extrinsic factors (including polymer residues [36]), leading to device-to-device variations [37]. Figure 8(a) gives an example of device-to-device variation with the signal strength at 0 pg ml^{-1} varying between the positive HBsAg and the negative BSA, even though the same PBS (pH7.4) buffer was used for both measurements. Grain boundaries are expected to be more reactive than the basal plane of the graphene and could accumulate absorbed molecules/particles & contaminants more readily [38]. In general, a combination of intrinsic & extrinsic factors is likely to contribute to differences in device-to-device signal response. Additionally, AuNP distribution and BSA blocker coverage on the graphene surface could

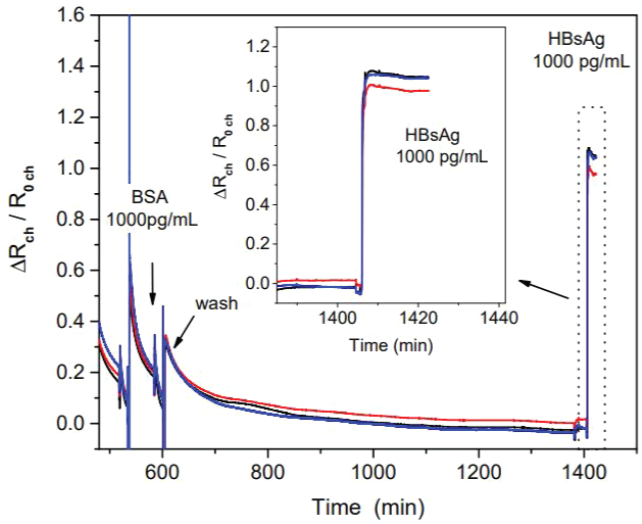

Figure 9. Graphene real-time measurement of channel resistances after application of BSA (1000 pg ml^{-1}) at time range less than 600 min, standard wash steps with N_2 drying, dry measurement between 600–1400 min and after HBsAg (1000 pg ml^{-1}) at 1400 min. The inset demonstrates the detailed time response to HBsAg application.

also contribute to variations in the device-to-device performance. Therefore, normalized resistances must be used.

Normalized resistances for all three channels are plotted against time for increasing HBsAg concentrations (figure 8(a) (top)). The measured graphene resistance was normalized using the resistance value measured at time t = 0. The same procedure was used to measure changes in response to BSA, as a negative control sample. A negative control protein was used to test for non-specific responses of the sensor and to control for any cumulative effects of the sequential testing regime. Normalized resistances for all three channels against time for increasing BSA concentrations are plotted in figure 8(a) (bottom). Figure 8(a) (top) shows a rise in $\Delta R_{ch}/R_{0\,ch}$ with increasing HBsAg indicating concentration dependence. The resistance was recorded as a function of time, the addition of HBsAg sees only a further increase in resistance, from that at the functionalization stage, suggesting a charge transfer of electrons to the graphene. In contrast, figure 8(a) (bottom) shows no concentration dependence for the negative control protein (BSA).

Normalized channel resistance plotted against log concentration of HBsAg is shown in figure 8(b), the lowest detection limit was determined as the intersection of the baseline at the lowest concentrations and the linear approximation of the experimental values at higher antigen concentrations. Both fitted lines are plotted through the average resistance values for the three channels. Taking into account the specific noise of the experimental data, the detection threshold is shifted to a higher concentration value, with an experimental LOD of 50 pg ml^{-1} (2.08×10^{-12} mol l^{-1}), this is comparable to current tests with LOD ranges between 0.04–0.62 ng ml^{-1} [39]. Similar results were observed for a further nine graphene channels.

To confirm that the negative response signals for the BSA control are true negative results and not a result of a faulty graphene device, HBsAg was added to the negative control sample device after all of the BSA concentrations had been applied. Following the final application of 1000 pg ml^{-1} BSA and standard wash steps, the sensor was allowed to relax overnight. 20 μl of 1000 pg ml^{-1} HBsAg was placed onto the channel window and incubated at room temperature for 15 min. In response to this, the relevant changes in channel resistances (figure 9) were remarkably different from the changes observed for the BSA negative control measurements. The introduction of HBsAg produced resistance changes similar to that observed for the HBsAg positive sample, figure 8(a) (top), demonstrating the specific detection of the HBsAg biomarker.

4. Conclusions

A graphene device has been demonstrated for real-time detection of HBsAg using a hybrid graphene-AuNP platform. Functionalized AuNPs were successfully decorated onto graphene via π–π stacking of ssDNA and part-hybridization of a graphene anchored ssDNA sequence with a ssDNA functionalized AuNP. The resultant dsDNA link creates the hybrid graphene-AuNP. Decoration of the graphene was observed with no attachment of particles to the SiO_2 surrounding substrate. Real-time 2-point resistance measurements showed each stage of functionalization produced an increase in resistance. HBsAg was successfully detected as an increase in $\Delta R_{ch}/R_{0\,ch}$ with increasing HBsAg concentration. A limit of detection of 50 pg ml^{-1} (2.08×10^{-12} mol l^{-1}) was observed. BSA was used as a negative control protein with no concentration dependence observed for the graphene resistor. The

graphene sensor was successfully demonstrated for the detection of HBsAg, acute and/or chronic biomarker for HBV. The platform may be used in future for detection of other biomarkers, making it an interchangeable and potentially universal platform for sensing applications.

Acknowledgments

This research was funded by Innovate UK under Newton Fund- China- UK Research and Innovation Bridges Competition 2015 (File Ref: 102877) and Knowledge Economy Skills Scholarships (KESS). The authors would also like to acknowledge Biovici Ltd. We acknowledge the inputs from YL through the joint project supported by the National Key Research and Development Program of China (Grant No. 2016YFC0101100 and 2016YFE0125200). ZT acknowledges the joint financial support of the Welsh Government and European Commission under the European regional Development funds (ERDF) through Sêr Cymru II Fellowships (project number: 80761-su-100)

The authors declare no conflicts of interest.

ORCID iDs

F Walters https://orcid.org/0000-0003-1732-6886
D Buckley https://orcid.org/0000-0002-5152-5443
Z Tehrani https://orcid.org/0000-0002-5069-7921
J Mitchell https://orcid.org/0000-0003-1377-725X
O Kazakova https://orcid.org/0000-0002-8473-2414

References

[1] da Silva E T S G, Souto D E P, Barragan J T C, de Giarola J F, de Moraes A C M and Kubota L T 2017 Electrochemical biosensors in point-of-care devices: recent advances and future trends *ChemElectroChem* **4** 778–94
[2] Kozel T R and Burnham-Marusich A R 2017 Point-of-care testing for infectious diseases: past, present, and future *J. Clin. Microbiol.* **55** 2313–20
[3] El-Serag H B 2012 Epidemiology of viral hepatitis and hepatocellular carcinoma *Gastroenterology* **142** 1264–73
[4] Taebi S, Keyhanfar M and Noorbakhsh A 2017 A novel method for sensitive, low-cost and portable detection of hepatitis B surface antigen using a personal glucose meter *J. Immunol. Methods* **458** 26–32
[5] Chung K H *et al* 2015 Hepatitis B surface antigen quantification across different phases of chronic hepatitis B virus infection using an immunoradiometric assay *Gut Liver* **9** 657–64
[6] Ambrosi A *et al* 2016 Graphene and its electrochemistry-an update *Chem. Soc. Rev.* **45** 2458–93
[7] Peña-Bahamonde J, Nguyen H N, Fanourakis S K and Rodrigues D F 2018 Recent advances in graphene-based biosensor technology with applications in life sciences *J. Nanobiotechnol.* **16** 1–17
[8] Li D, Zhang W, Yu X, Wang Z, Su Z and Wei G 2016 When biomolecules meet graphene: From molecular level interactions to material design and applications *Nanoscale* **8** 19491–509
[9] Georgakilas V *et al* 2012 Functionalization of graphene: covalent and non-covalent approaches, derivatives and applications *Chem. Rev.* **112** 6156–214
[10] Rösicke F *et al* 2017 Functionalization of any substrate using covalently modified large area CVD graphene *Chem. Commun.* **53** 9308–11
[11] Criado A, Melchionna M, Marchesan S and Prato M 2015 The covalent functionalization of graphene on substrates *Angew. Chem., Int. Ed. Engl.* **54** 10734–50
[12] Yin P T, Shah S, Chhowalla M and Lee K-B 2015 Design, synthesis, and characterization of graphene–nanoparticle hybrid materials for bioapplications *Chem. Rev.* **115** 2483–531
[13] Tang L, Wang Y and Li J 2015 The graphene/nucleic acid nanobiointerface *Chem. Soc. Rev.* **44** 6954–80
[14] Patil A J, Vickery J L, Scott T B and Mann S 2009 Aqueous stabilization and self-assembly of craphene sheets into layered bio-nanocomposites using DNA *Adv. Mater.* **21** 3159–64
[15] Yin P T, Kim T H, Choi J W and Lee K B 2013 Prospects for graphene-nanoparticle-based hybrid sensors *Phys. Chem. Chem. Phys.* **15** 12785–99
[16] Niu X, Zheng W, Yin C, Weng W, Li G and Sun W 2017 Electrochemical DNA biosensor based on gold nanoparticles and partially reduced graphene oxide modi fi ed electrode for the detection of Listeria monocytogenes hly gene sequence *J. Electroanal. Chem.* **806** 116–22
[17] Yang Y *et al* 2014 Enhanced charge transfer by gold nanoparticle at DNA modified electrode and its application to label-free DNA detection *ACS Appl. Mater. Interfaces* **6** 7579–84
[18] Khalil I, Julkapli N, Yehye W, Basirun W and Bhargava S 2016 Graphene–gold nanoparticles hybrid—synthesis, functionalization, and application in a electrochemical and surface-enhanced Raman scattering biosensor *Materials* **9** 406
[19] Bai S and Shen X 2012 Graphene-inorganic nanocomposites *RSC Adv.* **2** 64–98
[20] He F A, Fan J T, Song F, Zhang L M and Lai-Wa Chan H 2011 Fabrication of hybrids based on graphene and metal nanoparticles by *in situ* and self-assembled methods *Nanoscale* **3** 1182–8
[21] Min S K, Kim W Y, Cho Y and Kim K S 2011 Fast DNA sequencing with a graphene-based nanochannel device *Nat. Nanotechnol.* **6** 162–5
[22] Walters F and West M L 2019 Solid phase conjugate *WIPO patent* no. WO2018046934A1
[23] Chehel Amirani M and Tang T 2015 Binding of nucleobases with graphene and carbon nanotube: a review of computational studies *J. Biomol. Struct. Dyn.* **33** 1567–97
[24] Akca S, Foroughi A, Frochtzwajg D and Postma H W C 2011 Competing interactions in DNA assembly on graphene *PLoS One* **6** e18442
[25] Green N S and Norton M L 2015 Interactions of DNA with graphene and sensing applications of graphene field-effect transistor devices: a review *Anal. Chim. Acta* **853** 127–42
[26] Tripathi K and Driskell J D 2018 Quantifying bound and active antibodies conjugated to gold nanoparticles: a comprehensive and robust approach to evaluate immobilization chemistry *ACS Omega* **3** 8253–9
[27] Pollitt M J, Buckton G, Piper R and Brocchini S 2015 Measuring antibody coatings on gold nanoparticles by optical spectroscopy *RSC Adv.* **5** 24521–7
[28] Anfossi L, Baggiani C, Giovannoli C and Giraudi G 2009 Homogeneous immunoassay based on gold nanoparticles and visible absorption detection *Anal. Bioanal. Chem.* **394** 507–12
[29] De Puig H, Bosch I, Carré-Camps M and Hamad-Schifferli K 2017 Effect of the protein corona on antibody-antigen binding in nanoparticle sandwich immunoassays *Bioconjug. Chem.* **28** 230–8
[30] Malard L M, Pimenta M A, Dresselhaus G and Dresselhaus M S 2009 Raman spectroscopy in graphene *Phys. Rep.* **473** 51–87
[31] Ferrari A C and Basko D M 2013 Raman spectroscopy as a versatile tool for studying the properties of graphene *Nat. Nanotechnol.* **8** 235–46
[32] Lin L *et al* 2019 Towards super-clean graphene *Nat. Commun.* **10** 1912

[33] Mello M L S and Vidal B C 2012 Changes in the infrared microspectroscopic characteristics of DNA caused by cationic elements, different base richness and single-stranded form *PLoS One* **7** e43169
[34] Banyay M, Sarkar M and Gräslund A 2003 A library of IR bands of nucleic acids in solution *Biophys. Chem.* **104** 477–88
[35] Pinto H and Markevich A 2014 Electronic and electrochemical doping of graphene by surface adsorbates *Beilstein J. Nanotechnol.* **5** 1842–8
[36] Ishigami M, Chen J H, Cullen W G, Fuhrer M S and Williams E D 2007 Atomic structure of graphene on SiO_2 *Nano Lett.* **7** 1643–8
[37] Lipatov A *et al* 2014 Intrinsic device-to-device variation in graphene field-effect transistors on a Si/SiO_2 substrate as a platform for discriminative gas sensing *Appl. Phys. Lett.* **104** 013114
[38] Huang P Y *et al* 2011 Grains and grain boundaries in single-layer graphene atomic patchwork quilts *Nature* **469** 389–92
[39] Ocana S, Casas M L, Buhigas I and Lledo J L 2011 Diagnostic strategy for occult hepatitis B virus infection *World J. Gastroenterol.* **17** 1553–7